



THE UNIVERSITY *of* EDINBURGH

Edinburgh Research Explorer

Approved and investigational fluorescent optical imaging agents for disease detection in surgery

Citation for published version:

Rehman, S, Brennan, P, Lilienkamp, A & Bradley, M 2023, 'Approved and investigational fluorescent optical imaging agents for disease detection in surgery', *International Journal of Surgery*.
<https://doi.org/10.1097/JS9.0000000000000459>

Digital Object Identifier (DOI):

[10.1097/JS9.0000000000000459](https://doi.org/10.1097/JS9.0000000000000459)

Link:

[Link to publication record in Edinburgh Research Explorer](#)

Document Version:

Publisher's PDF, also known as Version of record

Published In:

International Journal of Surgery

General rights

Copyright for the publications made accessible via the Edinburgh Research Explorer is retained by the author(s) and / or other copyright owners and it is a condition of accessing these publications that users recognise and abide by the legal requirements associated with these rights.

Take down policy

The University of Edinburgh has made every reasonable effort to ensure that Edinburgh Research Explorer content complies with UK legislation. If you believe that the public display of this file breaches copyright please contact openaccess@ed.ac.uk providing details, and we will remove access to the work immediately and investigate your claim.



Approved and Investigational Fluorescent Optical Imaging Agents for Disease Detection in Surgery

Authors: Sonia Rehman^a (Sonia.Rehman@ed.ac.uk), Paul Brennan^b (Paul.Brennan@ed.ac.uk), Annamaria Lilienkampf^a (Annamaria.Lilienkampf@ed.ac.uk) and Mark Bradley^a (Mark.Bradley@ed.ac.uk).

- a) *School of Chemistry, The University of Edinburgh, Joseph Black Building, David Brewster Road, Edinburgh, EH9 3FJ, UK.*
- b) *Centre for Clinical Brain Sciences, The University of Edinburgh, Chancellor's Building, 29 Little France Crescent, Edinburgh, EH16 4SB, UK.*

Highlights

- Optical medical imaging is fast becoming useful tool within the clinical setting.
- Optical imaging agents allow for disease visualisation and monitoring based on molecular signatures.
- Fluorescently targeted imaging agents can provide surgeons within additional intraoperative guidance during resection of diseased tissue.
- This review gives and overview of fluorescent imaging agents currently utilised and in clinical trials to approve their use in a surgical setting.

Data Statement

This review article contains no original data. All data reviewed throughout this article can be found in the referenced articles or via the clinical trial identifier that are also referenced throughout.

Keywords: *optical medical imaging, fluorescence, intra-operative, surgical, real-time imaging, peptides*

Abstract

Fluorescent optical imaging is becoming an increasingly attractive imaging tool that physicians can utilise as it can detect previously ‘unseen’ changes in tissue at a cellular level that are consistent with disease. This is possible using a range of fluorescently labelled imaging agents that, once excited by specific wavelengths of light, can illuminate damaged and diseased tissues. For surgeons, such agents can permit dynamic, intraoperative imaging providing a real-time guide as they resect diseased tissue.

ACCEPTED

Introduction

Medicine evolved rapidly during the 20th century, with new procedures, revolutionary drugs and technologies. Among these are a suite of medical imaging techniques and procedures. Medical imaging relies on the old adage “seeing is believing”, except here the “belief” is really a confirmation that there is a need for treatment that may range from an administration of a drug to a surgical intervention, or indeed both, since current imaging scenarios do not lead to direct intervention in their own right. Current clinical imaging methods include MRI, PET, CT/X-ray, both pre and post intervention, but from a clinical standpoint there is huge unmet need as there is often little to monitor and to ‘see’ what is actually happening during the intervention. Now in the 21st century, opportunities such as optical medical imaging have begun to emerge that synergise the molecular basis of disease with fluorescent technologies. These provide imaging based on biomarkers that are disease dependant such that treatment and disease progression can be monitored at a cellular/molecular level. In addition, as optical molecular imaging techniques utilise the visible light spectrum, these imaging techniques not only reduce the need for exposure to radiation but offer exquisite molecular sensitivity.

Optical Medical Imaging

Optical imaging encompasses a suite of imaging modalities to visualise and indeed interrogate structures, cells and tissues through the use of the classical visible and deep red spectrum of light (400 to 900 nm). Examples of clinically relevant optical imaging modalities include endoscopy, optical coherence tomography (OCT), photoacoustic imaging and fluorescence¹. X-ray and PET are also optical imaging techniques, but this review will use the term “optical imaging” in relation to the more classical visible spectrum of light.

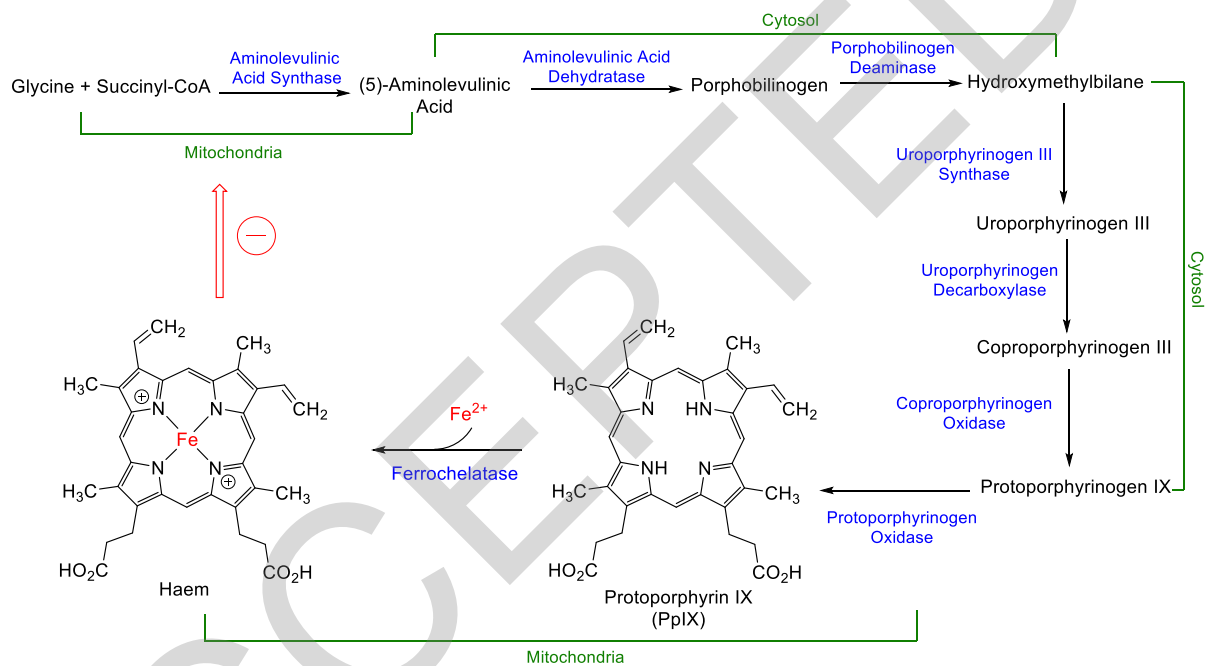
Optical imaging can allow the visualisation of disease at a molecular level and has begun to use a range of fluorescent techniques as a powerful tool for, not only disease diagnosis, but for following disease progression and treatment monitoring *e.g.*, imaging disease-dependant biomarkers. One particular area of interest in a clinical setting is fluorescence guided surgery, allowing surgeons to monitor and investigate molecular signatures consistent with disease as they operate in real-time². It is beneficial for patients and surgeons alike if fluorescence guided surgery can aid in delineating the margins of disease that can often be invisible/unclear and results in poor surgical margins, *i.e.*, surgeons under-cutting and leaving diseased tissue behind, the need for repeated surgery, or removal of healthy tissue and disfigurement.

Fluorescence imaging uses light emitted following excitation of a fluorescent compound. In the context of optical-based imaging within a clinical setting, fluorophores with emissions above 650 nm are more conducive to *in vivo* imaging as this avoids the background fluorescence or ‘noise’ that result from naturally occurring endogenous fluorophores such as porphyrins, tryptophan, reduced nicotinamides, flavins, lipo-pigments, and folate³. This review introduces fluorescent probes that are currently approved for use in the clinic or are in clinical trials and under investigation for fluorescence guided cancer surgery.

5-Aminolevulinic Acid (5-ALA)

5-Aminolevulinic acid (5-ALA) is used in glioma resection by neurosurgeons. It targets the haemoglobin biosynthesis pathway. 5-ALA is an endogenous metabolite generated from succinyl-CoA and glycine and is an intermediate along the haemoglobin biosynthesis pathway⁴. The biosynthesis pathway generates haem prior to the formation of haemoglobin (Figure 1).

Figure 1. Overview of haemoglobin biosynthesis pathway, showing the major metabolic steps and enzymes (in blue) to form haem prior to its conjugation to a protein to form haemoglobin. In healthy tissue, haem formation has a negative feedback effect on aminolevulinic acid synthase, allowing the cell concentrations of 5-ALA and, by extension, haem to be controlled^{5,6}. In cancerous tissue, a reduced ferrochelatase expression level results in a build-up of the PpIX intermediate that is fluorescent (emits at 635 nm when excited at 405 nm).

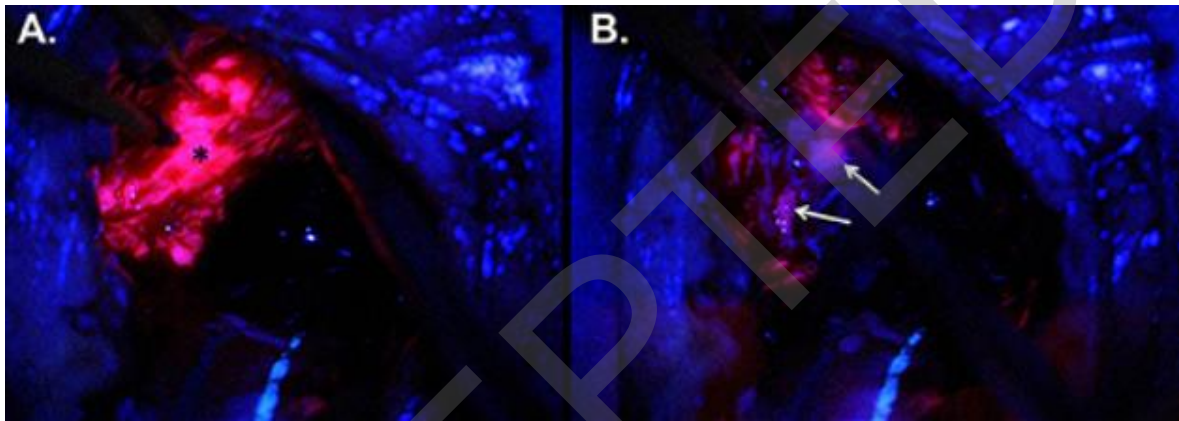


Along this pathway, fluorescent protoporphyrin IX (PpIX) (emits at 635 nm when excited at 405 nm) is formed in the step before haem formation. Within healthy cells, PpIX is metabolised by ferrochelatase to haem. Within glioma cells, there is a reduced level of ferrochelatase expression, resulting in both a build-up of fluorescent PpIX and a lack of negative feedback, which results in continual fuelling of 5-ALA into the haemoglobin biosynthesis pathway⁷. Additionally, the haemoglobin biosynthetic pathway is upregulated in high grade gliomas due to cells undergoing uncontrolled proliferation⁸.

5-ALA was approved in 2017 by the FDA for the visualisation and removal of high-grade gliomas (HGG, WHO Grade III or IV) in adults⁹, although it was in widespread use by neurosurgeons for many years prior to its approval. 5-ALA, when administered, is effective in “optically highlighting” more than 90% of HGG¹⁰. An example of the fluorescence emission from a tumour following PpIX accumulation from 5-ALA administration can be seen in Figure 2. Interestingly, a systemic review that collated results from multiple studies found that 5-ALA administration resulted in fluorescence in less than 25% of low-grade gliomas (LGG)¹¹. Commercially available 5-ALA (formulated as 5-aminolevulinic acid hydrochloride) is available for use with a recommended dose of 20 mg per kg of patients body weight¹².

More recently, 5-ALA has been used for photodynamic therapy (PDT) as a treatment option for cancers. PDT uses photosensitisers such as porphyrins, which, upon excitation, become activated and generate singlet oxygen (among other reactive oxygen species) in the proximity of cells. This drives apoptosis and cell death^{13,14}. 5-ALA has been investigated as a PDT treatment option for cancers including malignant glioblastomas, superficial bladder cancer and other neoplasias¹⁵. Current Phase II clinical trial is investigating 5-ALA as a form of PDT for benign dermal neurofibromas as well as other superficial skin cancers¹⁶.

Figure 2. Example of the fluorescence imaging capabilities of 5-ALA (administered as 5-ALA hydrochloride) in visualising a high-grade glioma 5-ALA imaging helps tumour identification (in pink) and delineation of surrounding healthy tissue (in blue). Areas of dense, necrotic tissue in the tumour core that are no longer metabolising are unable to generate/accumulate the fluorescent PpIX. Proliferating solid tumour (in A annotated by*) and regions of diffuse tumour infiltration (in B indicated by white arrows) where margins are unclear are demonstrated in the image above¹⁷ (left). Image reproduced from open access article¹⁷ with permission from Frontiers Media.

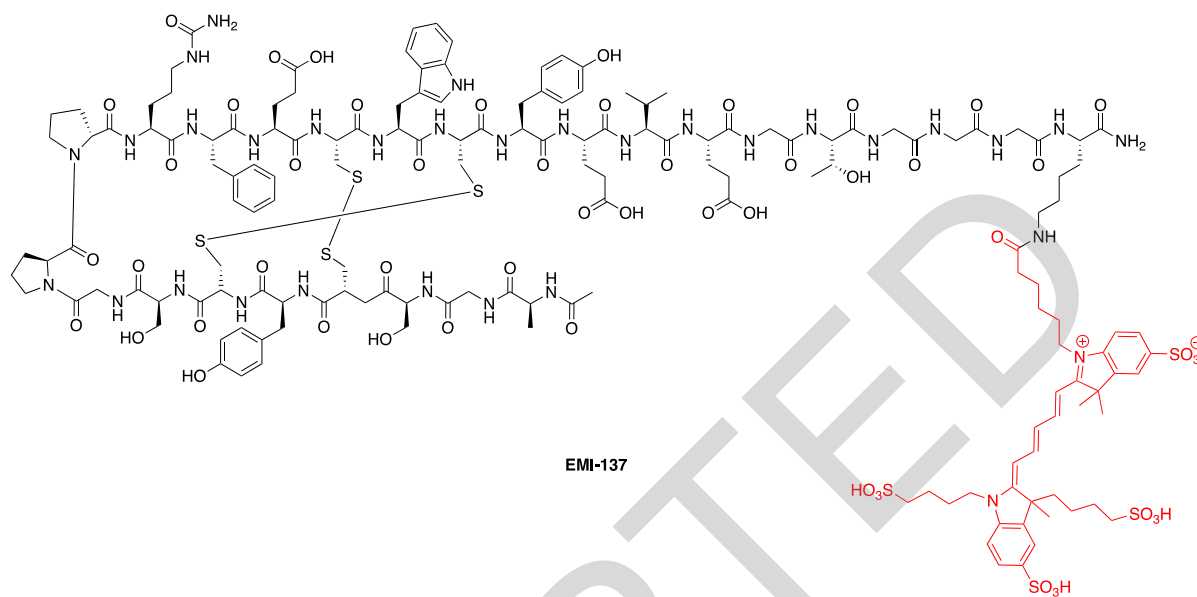


EMI-137

c-MET (as Hepatocyte Growth Factor Receptor (HGFR)) binds the Hepatocyte Growth Factor (HGF), a plasminogen-like protein. Once bound to c-MET receptors, HGF mediates cellular repair and regeneration in healthy tissue^{18,19}. The c-Met receptor is part of the tyrosine kinase family of receptors from the MET gene family. c-MET receptors have been implicated in a number of cellular pathways including cell signalling, proliferation, growth, development, migration and invasion within the context of cancer²⁰. Over expression of the c-MET receptor has been found in the tumour growth and development stages (specifically angiogenesis, cell invasion and metastasis stages of tumour growth) of cancers and other diseases including glioblastoma, Barrett's oesophagus, colorectal cancer and colitis^{21,22}.

EMI-137 (also called GE-137) is a Cy5 fluorophore labelled multi-cyclic peptide that binds c-Met, which is overexpressed in cell membranes within diseased colon tissue. This peptide ligand was discovered from phage display/selection where several peptides were identified that had different sequences and modes of function. Thus, some peptides showed binding to c-MET and inhibited HGF binding, other peptides were shown to bind at another site on the c-MET receptor, allosterically inhibiting HGF binding²³. The peptide AGSCYCSGPPRFECWCYETEGT (containing two intramolecular disulphide bridges) showed good binding affinity to the c-MET receptor ($K_d = 3$ nM) and was found to bind to a site on the receptor that did not impinge on HGF binding and was thus selected for further studies²³. EMI-137 is composed of a *bis*-disulphide 22-mer c-MET targeting peptide, with a C-terminal primary amide and an acetylated amino terminus, while a GGGK spacer allows conjugation of the NIR Cy5** fluorophore (Ac-AGSCYCSGPPRFECWCYETEGT-GGGK(Cy5**)-NH₂)²⁴ and separation of the dye from the targeting peptide (Figure 3). The Cy5** fluorophore used gives the probe excitation and emission wavelengths of 650 nm and 669 nm (the Cy5** nomenclature depicts its multiple sulfonations that promotes its solubility).

Figure 3. Chemical structure of EMI-137 showing the disulphide bridges between cysteine residues 4-16 and 6-14. The Cy5** fluorophore (in red), bearing four sulfonate groups to promote solubility, is conjugated to the targeting peptide via a small peptide spacer (GGGK).

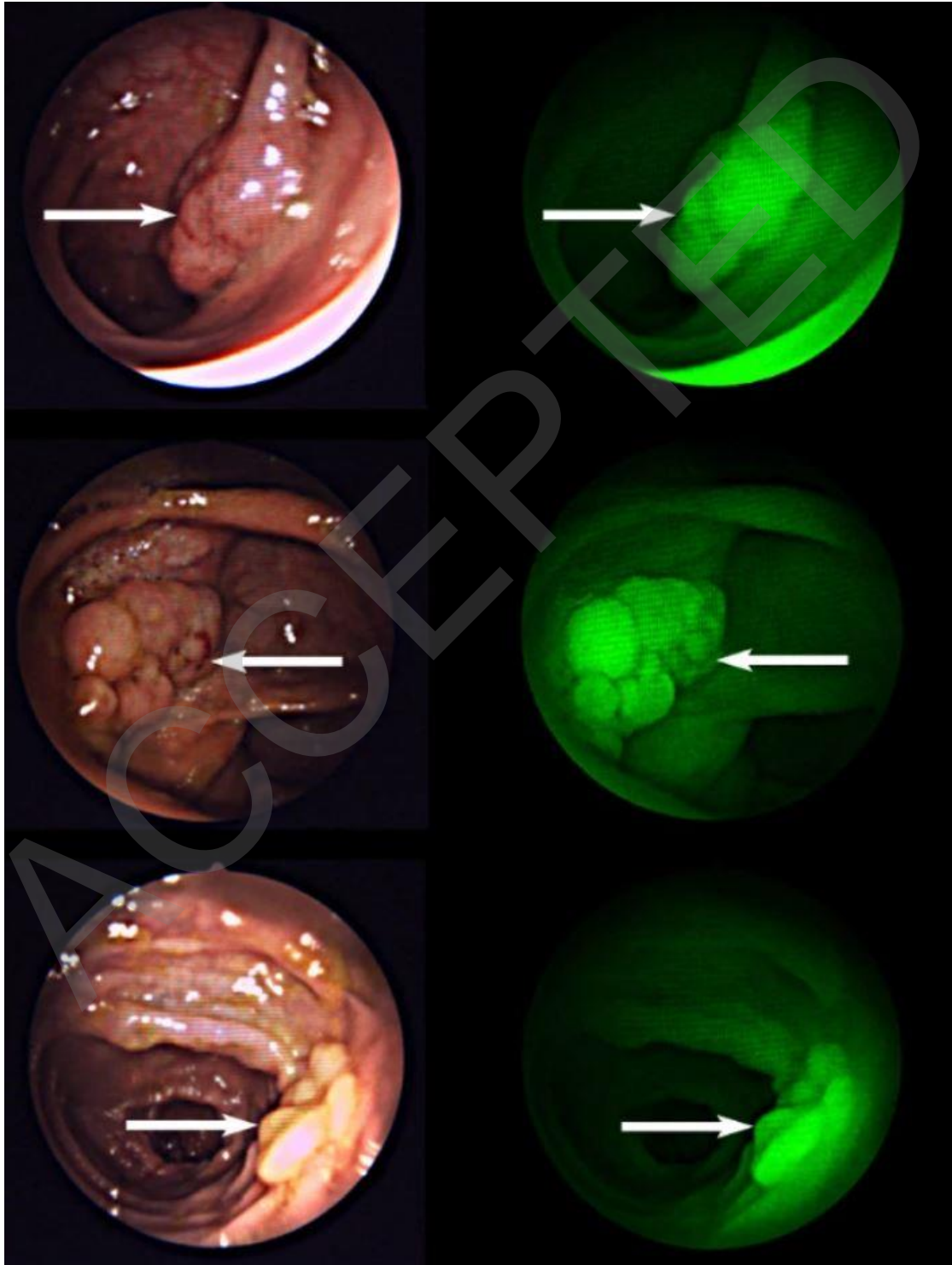


ACCEPTED

EMI-137 has been investigated to image colorectal polyps that are found to be a prominent pathological feature of colorectal cancer, colitis and Crohn's disease²⁵. The inflammatory nature of colorectal polyps makes visualisation by colonoscopy or exploratory surgery difficult as polyps are often surrounded by inflamed bowel tissue that can disguise diseased tissue. Intravenous administration of EMI-137 target overexpressed c-MET receptors in the polyps allowing visualisation of polyps when excited at 650 nm (using a custom designed/built system) during colonoscopy. The identification of bowel polyps using fluorescent EMI-137 compared to standard white light colonoscopy can be seen in Figure 4.

ACCEPTED

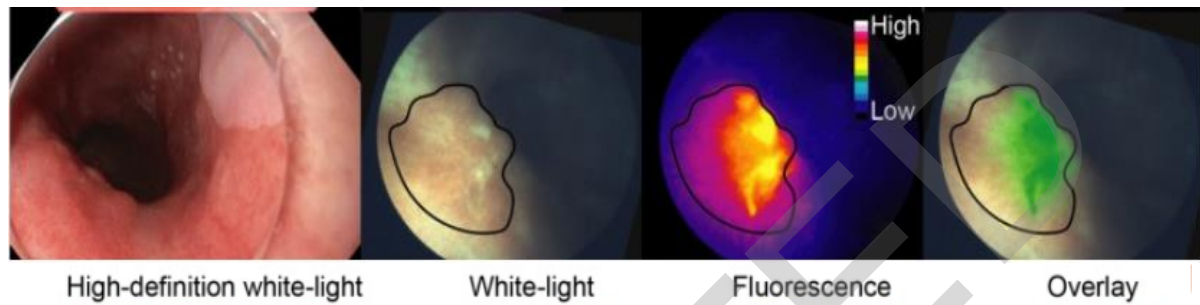
Figure 4. Images from colonoscopy of bowel colorectal polyps when the patient has been administered with EMI-137. Images on the left show the comparison of visualisation using standard white light (in the field of view in an endoscopy/colonoscopy) compared to the fluorescent images (in green) showing ‘unseen’ polyps that were not as evident in white light from the application of EMI 137²⁴. Image reproduced from article²⁴ with copyright permission granted from Springer Nature.



EMI-137 is currently in Phase IIb clinical trials for the identification, detection and screening of colorectal polyps and cancers. Studies include the investigation of whether EMI-137 is capable of producing fluorescence and detecting primary tumours (that are confirmed to be c-MET positive by histology) whilst developing an *in vivo* safety profile, with studies also exploring whether EMI-137 can detect cancer draining lymph nodes where metastasis has been confirmed by histological studies²⁶. EMI-137 has also been investigated in a Phase I trial for detection of Barrett's oesophagus – a pre-cancerous disease. When compared to standard white light, EMI-137 localisation to lesions was found to provide a gradient of visualisation of expressed c-MET receptors (Figure 5) that could allow targeted treatment within the area of dense fluorescence. In this investigation, EMI-137 was administered intravenously at up to 0.13 mg per kg of body weight²⁶.

ACCEPTED

Figure 5. Comparison of traditional “white light” imaging and fluorescence imaging (excitation at 650 nm) with an overlay of images of the inflamed oesophagus when EMI-137 was administered IV. The overlay highlights (in green) where EMI-137 has concentrated likely where there is increased c-MET receptor expression²⁷. Image reproduced from open access article²⁷ with permission from Ivyspring International.

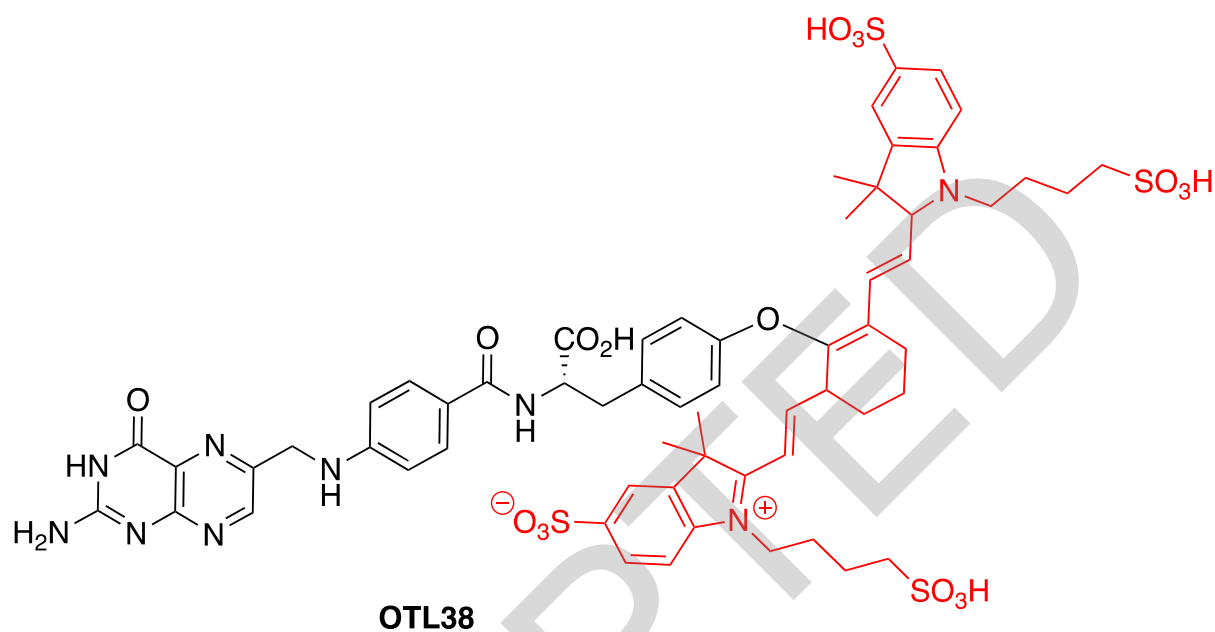


ACCEPTED

OTL38

OTL38 is a near infrared (NIR) imaging probe based on folic acid coupled to an indole cyanine-like green dye (SO456) (Figure 6). In synthesising this probe, the glutamic acid residue of folate was replaced with a tyrosine that was *O*-alkylated with the SO456 dye^{28, 29}. The replacement of the glutamate by tyrosine gives an increase in fluorescence intensity by more than 200% (when compared to the SO456 dye alone). It is thought that the conjugation of the tyrosine to the meso-chloride of SO456 contributed to the system of electron delocalisation and thus brought about the noted fluorescence intensity²⁹. OTL38 is excited at 776 nm and emits at 793 nm.

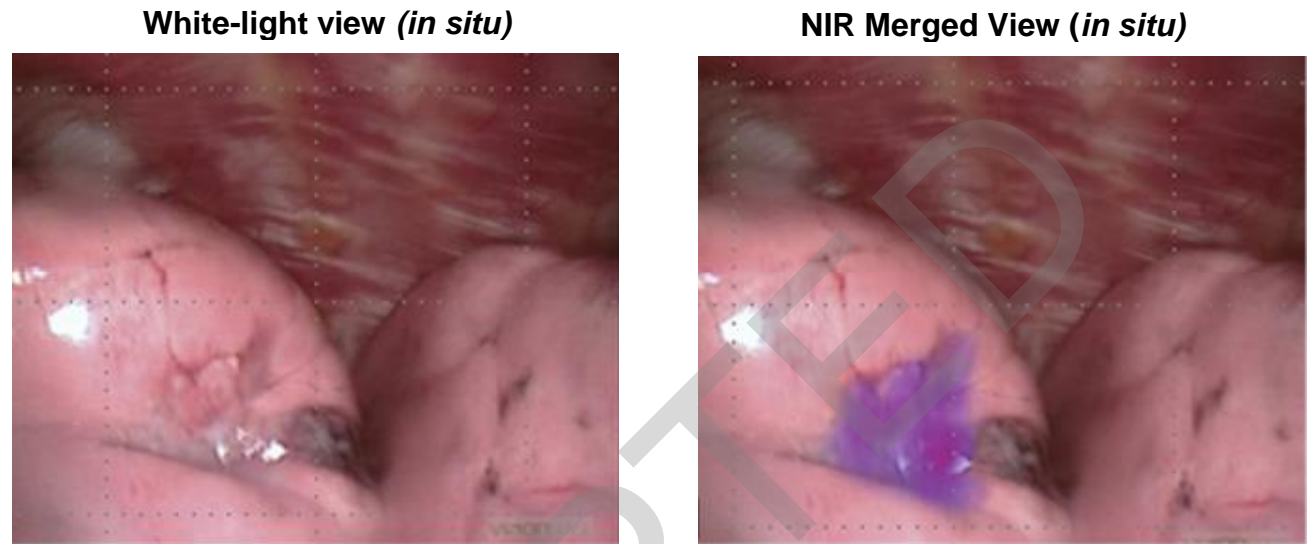
Figure 6. Chemical structure of probe OTL38 where a folate-type ligand is conjugated to the SO456 indole-like NIR dye (in red) via a tyrosine residue.



OTL38 targets the folate receptor alpha (FR α) overexpressed in several cancers. More than 80% of ovarian tumours³⁰ and 74% of pulmonary adenocarcinomas³¹ have increased FR α expression³². FR α , expressed by the FOLR1 gene, is typically activated and expressed in early embryonic development³³, thus, in the context of healthy tissue, there is low FR α expression but increased expression observed in cancerous tissue³⁴. Activation of FR α is thought to be involved in episodes of rapid cellular proliferation with folate binding supporting DNA synthesis prior to mitotic division^{33, 35}. With high levels in diseased tissue and low levels in healthy tissue, FR α is an attractive biomarker for imaging ovarian and lung cancer. OTL38 was approved by the FDA in 2021 as Pafolacianine after its Phase III clinical trials for the intraoperative identification, imaging and resection of FR α positive ovarian and lung cancers provided promising clinical data^{36, 37}. Additionally, a dose guidance of up to 0.025 mg per kg of body weight was also advised. This was advised to be administered as a continuous intravenous infusion over 60 minutes up to 9 hours before surgery³⁸. An example of the imaging capabilities of OTL38 from Phase II studies are shown in Figure 7.

ACCEPTED

Figure 7. Comparison of *in situ* tumour visualisation of pulmonary squamous cell carcinomas in white light alone (left) and by merge of observed OTL38 fluorescence at 776 nm. Overlaying OTL38 signal provides localisation of FR α +ve tumour tissue to allow for focused resection of diseased tissue³⁹. Image reproduced from open access article³⁹ with permission from Elsevier.

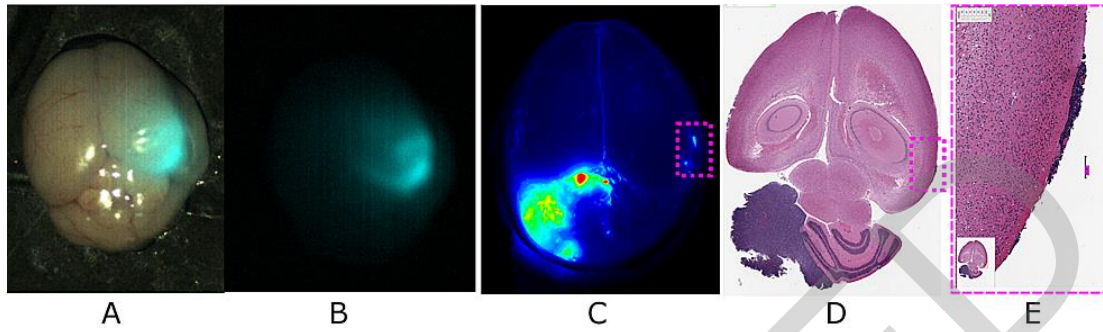


BLZ-100

BLZ-100 (one of the compounds in the Tumour Paint series by Blaze Bioscience) has potential for use in surgical resections of solid mass tumours^{40,41}. BLZ-100 consists of a chlorotoxin (CTX) peptide to which the fluorophore indocyanine green (ICG) has been attached via NHS ester formation – this results in a NIR probe with an excitation/emission of 675 nm/740 nm, whilst ICG alone has an excitation/emission of 789 nm/814 nm (see section on ICG). The use of ICG as a NIR fluorescent dye in BLZ-100 allows for an ease of accessibility in using this probe as its emission window can be imaged using existing and currently available optical imaging hardware currently used in clinical environments. BLZ-100, when intravenously administered was found to be safe for use at a dosage of up to 30 mg per kg of body weight in Phase I Safety and Pharmacokinetic investigations⁴¹. Currently, BLZ-100 is in several Phase I clinical trials for use in skin, brain and breast tumours, and in Phase II and III clinical studies for paediatric central nervous system tumours⁴². BLZ-100 has been fast tracked by the FDA for paediatric central nervous system tumours.

Chlorotoxin (CTX) is 36mer peptide (MCMPCFTTDHQMARKCDDCCGGKGRGKCYGPQCLCR) with 8 cysteines forming 4 disulphide bonds and making it structurally very compact and protease resistant^{43,44}. It was initially isolated from scorpion venom of *Leiurus quinquestriatus* and binds to chloride ion channels. Chloride ion channels are overexpressed in cancers such as glioblastoma, lung and skin cancer. In the context of cancer, chloride ion channel over activity can result in a regulatory volume decrease in cells that can be brought about due to hypotonic stress⁴⁵. Regulatory volume decrease contributes to phenotypic changes seen in cancer development at a cellular level and can cause changes in cell shape and increase cellular migration⁴⁵. Chloride ions and channels also act as co-transporters for potassium ions whose influx is known to be implicated in tumorigenesis. CTX's tumour binding capabilities were first investigated in rat glioblastoma models where CTX was found to bind to gliomas, but interestingly did not bind to healthy rat astrocytes⁴³. CTX has therefore become an attractive targeting ligand in tumour binding studies. The focus of BLZ-100's glioblastoma identification and delineation in mice brains showed fluorescence at probe concentrations as low as 500 pM with BLZ-100 showing no binding or fluorescence in healthy mice brain tissue (containing a cross section of neuronal and astrocyte cells (Figure 8)⁴⁶.

Figure 8. A-B) injected BLZ-100 on whole mouse brain imaged using a clinical prototype imaging system ‘SIRIS’ system with tumour highlighted; C) whole mouse imaging of IV BLZ-100 with peripheral tumour cells highlighted; D-E) histological staining showing tumour tissue⁴⁶. Image reproduced from open access article⁴⁶ with permission from Cureus.



A

B

C

D

E

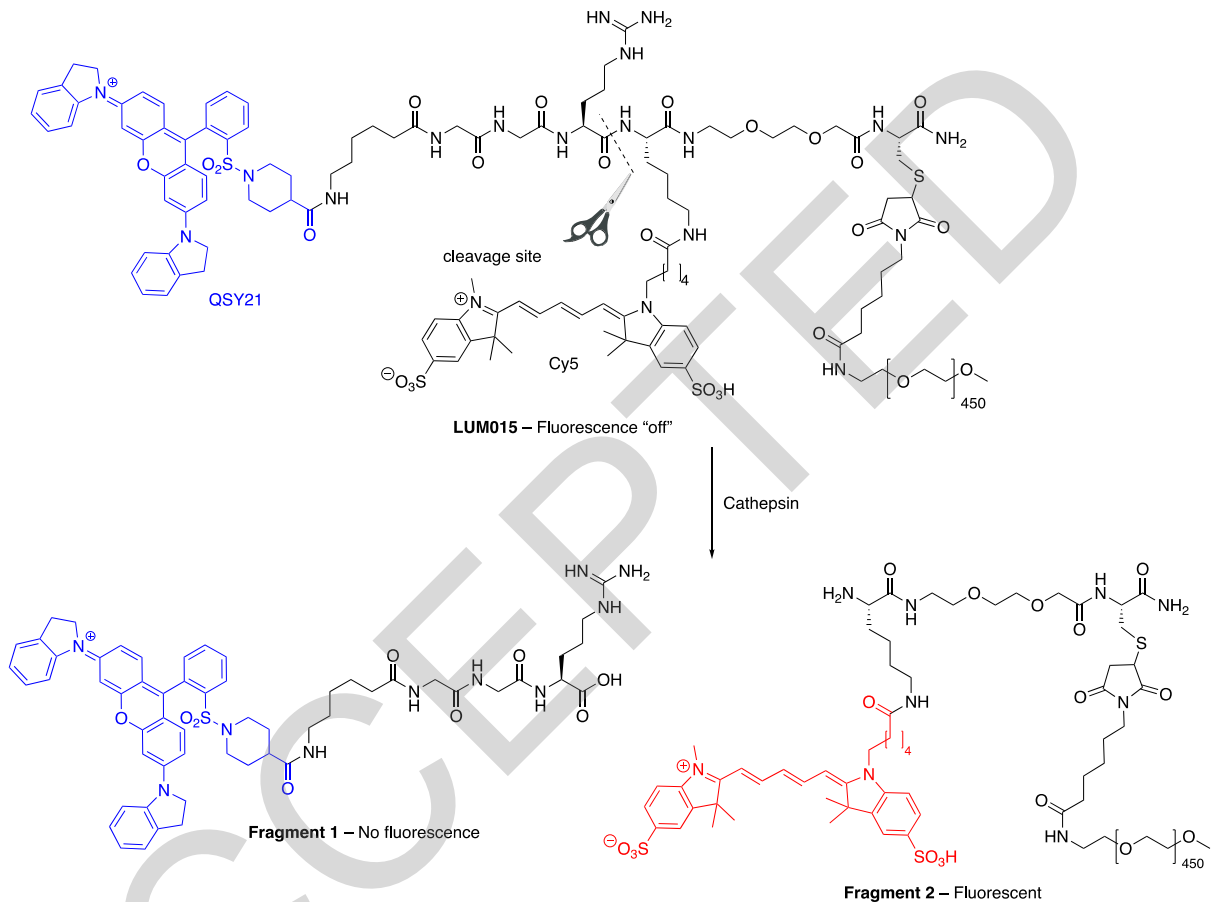
ACCEPTED

LUM015

Cathepsins are a class of cysteine proteases with a wide range of activities and are specifically noted for their involvement in remodelling type II, IX and XI collagens and proteoglycans. Their activity is regulated by cytokine signalling and Ras proto-oncogene expression, with mutations in the Ras proto-oncogene associated with 70% of colorectal cancers and 47% of carcinomas⁴⁷. The overexpression of multiple types of cathepsins has been linked to the development and progression of many cancers, with overexpression enabling cancer progression by aiding cell proliferation, tissue modelling and angiogenesis, tumour growth and cellular metastasis⁴⁸. Cathepsins B in particular has been associated with invasive and metastatic phenotypes typically found in aggressive forms of cancer.

LUM015 has been described as an ‘onco-fluorescent’ and protease-cleavable deep-red probe⁴⁹, which fluorescence is quenched until cleaved/activated. It consists of the quencher QSY21 attached to the N-terminus of a small peptide (sequence GGRK), with the C terminus linked to a 20kD PEG unit. QSY21 acts a quencher for the Cy5 fluorophore (FRET pair) attached to the lysine side chain (QSY21-GGRK(Cy5)-PEG-OMe)^{50,51}. The addition of the PEG unit promotes tumour accumulation when administered intravenously⁵². This probe was designed to target the microenvironment around tumours and becomes optically active in the present of cathepsins and matrix remodelling⁴⁹ with cleavage of the Arg-Lys bond by cathepsins K, L, S and B (Figure 9) liberating the Cy5 fluorophore (excitation and emission wavelengths are 649 nm and 670 nm). LUM015 is currently in Phase III clinical trials for intraoperative use in detecting residual breast cancer tissue in patients undergoing standard lumpectomy⁵³. This study administered LUM015 to patients intravenously up to 6 hours prior to lumpectomies at a dose of 1.0 mg per kg of body mass. Imaging of tumour masses was carried out using the Lum System for intraoperative imaging and guidance⁵³.

Figure 9. The structure of the FRET-based LUM015 and the fragments resulting from cathepsin cleavage at the Arg–Lys amide bond. Fragment 1 contains the QSY21-GGR. Fragment 2 is composed of the fluorescent Cy5 dye attached to the 40kD PEG chain via the lysine residue, whilst Fragment 3 is Lys-Cy5 where the PEG chain has been cleaved. Fragment 1 is optically inactive when excited at 649 nm, whilst Fragments 2 and 3 emit at 670 nm.



Indocyanine Green (ICG)

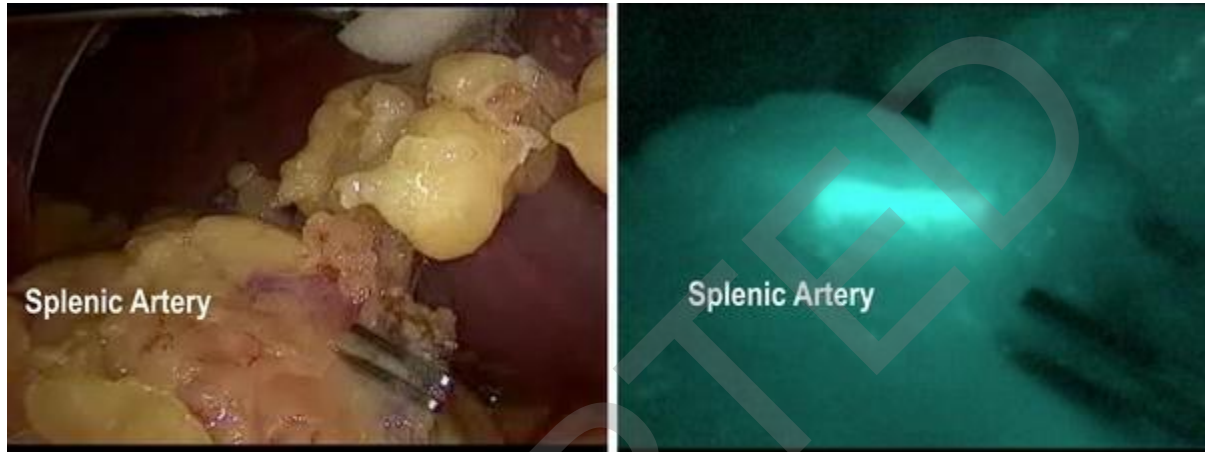
Indocyanine Green (ICG), as the name suggests, is a tricyanocyanine dye available in both sulfonated and non-sulfonated forms. The sulfonated dye is used clinically as it is freely soluble in water giving rise to a green solution that fluoresces in the NIR-I window (700-900 nm) with an excitation and emission maxima of 784 nm and 814 nm respectively (although these values are subject to small changes dependant on the dye's environment).

Early recorded use of ICG date back to the late 1950s where it was used in the study of cardiac blood flow⁵⁴. Investigation found that once administered, the dye was both rapidly distributed (is this the sulfonated or the non-compound) and cleared with more than 97% of the loading dose demonstrating hepatic excretion via the bile duct with little to no alteration of the dye's structure⁵⁵. In its native form, ICG is untargeted (unlike, for example, BLZ-100) and shows low toxicity (LD₅₀= 80mg/kg) – a property that stems from its lack of binding and rapid clearance with half-life of only 4 minutes⁵⁶.

Use of intravenously administered ICG includes angiography, where the dye provides blood vessel contrast that may be subject to occlusion, damage or trauma and for assessing intraoperative myocardial perfusion⁵⁷, with an example of the imaging capability of ICG in viewing vascular anatomy shown in Figure 10⁵⁸. Typical dosages required for angiography can range from 0.1 to 5.0 mg/kg and are highly dependent on the clinical investigation⁵⁹.

ACCEPTED

figure 10: Comparison of the splenic artery provided by standard white light (left) and ICG fluorescence (right). ICG diluted in saline was administered intravenously and imaged using ICG-Pulsion by Pulsion Medical System. In the presence of ICG, visualisation at 800 nm provides a more readily defined splenic artery outline than white light alone. Image reproduced from open access article⁵⁸ with permission from Springer Nature.



ACCEPTED

Importantly the emission window of ICG also extends into the near-infrared-II window (NIR-II 1000 nm – 1700 nm). This has proven to be clinically important as NIR-II light undergoes reduced scattering with tissue ($-\lambda^4$) with lower levels of auto fluorescence than in the visible or NIR-I region. In addition, studies have demonstrated that with a disrupted blood-brain barrier ICG can accumulate in GBM⁶⁰. Recent examples have shown that ICG use with visualisation in the NIR-II window have yielded promising results. In a first-in-human investigation assessing tumour detection using a multi-spectral imaging system. It was found here that when administering ICG in patients with confirmed metastatic liver tumour, NIR-II had a higher tumour detection sensitivity rate than NIR-I imaging (100% compared to 90.6% respectively)⁶¹. A similar finding was reported by Shi *et al*⁶² who compared the effectiveness of high grade glioma detection and resection between NIR-II (using ICG) and conventional white light surgical guidance. Here, it was demonstrated that NIR-II ICG fluorescence guided surgery had a higher accuracy rate in detecting tumour tissue than white light detection (97.0% to 80.5%). This comparison was carried out using data from intraoperative guidance as well as ex-vivo imaging to compare resected tumour tissue to surrounding healthy tissue margins⁶². The use of ICG within the context of the brain is particularly interesting as could provide useful in the investigation of not only tumour tissue, but also potentially of blood flow in microvasculature given its ability to bypass a disrupted blood-brain-barrier.

ACCEPTED

Table 1: Summary of imaging agents discussed in the review (both FDA approved and investigational new drugs) highlighting the disease type, area targeted by probe, structure type, approval status, optical properties and reported dosage.

Imaging Agent	Disease	Target	Structure-type	Approval Status	Optical properties (wavelength of excitation/emission)	Reported dose
5-ALA (4, 10, 16)	High grade glioma imaging and resection	Haem biosynthesis pathway	Small molecule that is incorporated into the haem biosynthesis pathway	FDA approved for use in high grade gliomas.	405/635 nm	20 mg per kg (administered as Gliolan)
EMI-137 (25,26)	For use in imaging in colorectal, breast, head and neck and lung cancer	Overexpressed c-MET receptors	22 mer peptide labelled with Cy5**	Currently in Phase IIb clinical trials for colorectal cancer and Phase I for breast and head and neck	650/669 nm	0.13 mg per kg
OTL38 (28, 30, 38)	Indicated for use in imaging of ovarian cancer for surgical resection	Targets overexpressed FR α present in tumour tissue	Small molecule targeting FR α coupled to a NIR dye	Gained FDA approval for use in imaging of ovarian cancer (Pafolacianine) in 2021	776/793 nm	0.025 mg per kg (administered as Pafolacianine)
BLZ-100 (41,42, 43)	Highlights brain and CNS solid state tumours	Binds to chloride ion channels overexpressed in tumours	Cyclic peptide derived from chlorotoxin coupled to ICG (a NIR dye)	In Phase II and III clinical trials for visualisation of brain and CNS tumours	675/740 nm	30.0 mg per kg
LUM015 (49, 51,	Labels breast cancer	Cathepsins present in higher	Peptide sequence exhibits	Phase III clinical trial	649/670 nm	1.0 mg per kg

53)	tissue for imaging during surgical resection	concentrations in cancer	fluorescence once cleaved by cathepsins	investigations underway		
ICG (54, 55, 59)	Perfusion based investigations and tumour detection	ICG has no binding target	Tricarbocyanine dye (available in sulfonated and non-sulfonated form)	Initial FDA approval granted in 1959	784/814 nm	0.1-5.0 mg per kg (dependent on investigation)

ACCEPTED

The Future of Optical Imaging in Surgery

Fluorescent optical medical imaging is a powerful technology just beginning to show glints of its full potential within the clinical arena – Table 1 provides a brief overview of the imaging agents discussed within this review. There are many other imaging probes under investigation yet to enter human studies and surgeons will be called upon to develop the use cases and evidence of clinical validity. We have highlighted applications in cancer but there will be broader application in surgery, infection monitoring, and disease diagnosis and monitoring as well as cancer margin delineation – all areas that are under active investigation. As an example, optical probe NP41, a peptide based reagent composed of a Cy5 fluorophore coupled to a nerve targeting peptide⁶³ highlights myelin encased nerves. NP41 could help identify nerves intra-operatively for preservation^{64,65}. A range of fluorescent molecules have been designed for imaging fungi (e.g. fluorescent Amphotericin B-based probes⁶⁶) or bacteria which could aid removal of infected tissue. As imaging technologies and detectors become ever more sophisticated fluorescent imaging that moves beyond the traditional optical window has advantages. For example, there is reduced light scattering by tissue at longer wavelengths and in this review dyes operating beyond 1000 nm show much promise. In addition, the value of newer imaging modalities, such as fluorescent lifetime, in which the long-known, intrinsic, fluorescent lifetime variation between healthy and diseased tissue offers huge promise in cancer margin determination, perhaps linked to other optical methods such as Raman. Optical medical imaging is a powerful technology and its application will support surgeons and robotic surgery in diagnosis, localisation and treatment of disease.

References

1. National Institute of Biomedical Imaging and Engineering. Optical Imaging. <https://www.nibib.nih.gov/science-education/science-topics/optical-imaging> [accessed March 2022].
2. Leitgeb RA, Baumann B. Multimodal Optical Medical Imaging Concepts Based on Optical Coherence Tomography. *Front in Phys.* 2018; 6; 114. DOI: 10.3389/fphy.2018.00114
3. Croce AC, Bottiroli G. Autofluorescence spectroscopy and imaging: a tool for biomedical research and diagnosis. *Eur J Histochem.* 2014; 58; 4. DOI: 10.4081/ejh.2014.2461
4. Saito K, Fujiwara T, Ota U, *et al.* Dynamics of absorption, metabolism, and excretion of 5-aminolevulinic acid in human intestinal Caco-2 cells. *Biochem Biophys Rep.* 2017; 13; 11: p.105-111. DOI: 10.1016/j.bbrep.2017.07.006
5. Brody T. Inorganic Nutrients. *Nutritional Biochemistry (Second Edition)*. Academic Press; 1999, p. 693-878.
6. Bhagavan N, Ha, C. Metabolism of Iron and Haem. *Essentials of medical biochemistry (Second Edition)*. Amsterdam: Elsevier Academic Press; 2015, p. 511-529.
7. Kondo M, Hirota N, Takaoka T, Kajiwara M. Heme-biosynthetic enzyme activities and porphyrin accumulation in normal liver and hepatoma cell lines of rat. *Cell Biol Toxicol.* 1993; 9; 1: p.95-105. DOI: 10.1007/BF00755143
8. Ross JL, Cooper LAD, Kong J, *et al.* 5-Aminolevulinic Acid Guided Sampling of Glioblastoma Microenvironments Identifies Pro-Survival Signalling at Infiltrative Margins. *Sci Rep.* 2017; 7: 15593. DOI: 10.1038/s41598-017-15849-w
9. Hadjipanayis CG, Stummer W, Sheehan JP. 5-ALA fluorescence-guided surgery of CNS tumours. *J Neurooncol.* 2019; 141;3: p. 477-478. DOI: 10.1007/s11060-019-03109-y
10. Hadjipanayis CG, Widhalm G, Stummer W. What is the Surgical Benefit of Utilizing 5-Aminolevulinic Acid for Fluorescence-Guided Surgery of Malignant Gliomas? *Neurosurgery.* 2015; 77; 5: p. 663-673. DOI: 10.1227/NEU.0000000000000929
11. Makkawi AK, El Almadieh TY, Wu EM, *et al.* The Use of 5-Aminolevulinic Acid in Low-Grade Glioma Resection: A Systematic Review. *Operative Neurosurgery.* 2019; 19; 1: p. 1-8. DOI: 10.1093/ons/opz336

12. National Institute for Health and Care Excellence. Brain Tumours (primary) and Brain Metastases in over 16s. <https://www.nice.org.uk/guidance/ng99> [accessed March 2022].
13. Mahmoudi K, Garvey KL, Bouras A, *et al.* 5-aminolevulinic acid photodynamic therapy for the treatment of high-grade gliomas. *J Neurooncol.* 2019; 141; 3: p. 595-607. <https://doi.org/10.1007/s11060-019-03103-4>
14. Inoue K. 5-Aminolevulinic acid-mediated photodynamic therapy for bladder cancer. *Int J Urol.* 2017; 24; 2: p. 97-101. DOI: 10.1111/iju.13291
15. Ishizuka I, Abe F, Sano Y, *et al.* Novel development of 5-aminolevulinic acid (ALA) in cancer diagnoses and therapy. *Int Immunopharmacol.* 2011; 11; 3: p. 358-365. DOI: 10.1016/j.intimp.2010.11.029
16. Whelan H. Photodynamic Therapy for Benign Dermal Neurofibromas – Phase II. ClinicalTrials.gov. Identifier: NCT02728388. Updated January 4, 2023. Accessed April 2022. <https://clinicaltrials.gov/ct2/show/NCT02728388>.
17. Maragos GA, Schüpfer AJ, Lakomkin N *et al.* Fluorescence-Guided High-Grade Glioma Surgery More Than Four Hours After 5-Aminolevulinic Acid Administration. *Front. Neurol.* 2021; 12: 644804. DOI: 10.3389/fneur.2021.644804.
18. Bottaro D, Rubin JS, Faletto DL, *et al.* Identification of the hepatocyte growth factor receptor as the c-met proto-oncogene product. *Science.* 1991; 251; 4995: p.802-804. DOI: 10.1126/science.1846706
19. Cheng F, Guo D. MET in glioma: signalling pathways and targeted therapies. *J Exp Clin Cancer Res.* 2019; 38; 270. DOI: 10.1186/s13046-019-1269-x
20. Organ SL, Tsao MS. An overview of the c-MET signalling pathway. *Ther Adv Med Oncol.* 2011; 3: p.S7-S19. DOI: 10.1177/1758834011422556.
21. Krause DS, Van Etten RA. Tyrosine Kinases as Targets for Cancer Therapy. *N Engl J Med.* 2005; 353: p.172-187. DOI: 10.1056/NEJMra044389.
22. Sierra JF, Tsao MS. c-MET as a potential therapeutic target and biomarker in cancer. *Ther Adv Med Oncol.* 2011; 3; 1: p.S21-S35. DOI: 10.1177/1758834011422557.
23. Dransfield DT, Ladner RC, Nanjappan P, Sato AK, inventors: Takada Pharmaceutical Co Ltd, assignee. Peptides that specifically bind HGF receptor (cMet) and uses thereof. Australian patent: AU2010235865B2. November 15, 2012.

24. Burggraaf J, Kamerling IM, Gordon PB, *et al.* Detection of colorectal polyps in humans using an intravenously administered fluorescent peptide targeted against c-Met. *Nat Med.* 2015; 21; 8: p.955-961. DOI: 10.1038/nm.3641
25. Colucci P, Yale SH, Rall CJ, *et al.* Colorectal Polyps. *Clin Med Res.* 2003; 1; 3: p.261-262. DOI: 10.3121/cm.1.3.261
26. Jayne D. EMI-137 in Laparoscopic Colonic Resections. ClinicalTrials.gov. Identifier: NCT03360461. Updated October 15, 2018. Accessed April 2022. <https://clinicaltrials.gov/ct2/show/NCT03360461>
27. De Jongh SJ, Voskuil F, Schmidt I, *et al.* C-Met targeted fluorescence molecular endoscopy in Barrett's esophagus patients and identification of outcome parameters for phase-I studies. *Theranostics*, 2020; 10; 12: p.5357-5367. DOI: 10.7150/thno.42224
28. Low PS, Kularatne SA, Kelderhouse LE, inventors: Purdue Research Foundation, assignee. Methods of Imaging Inflammatory Diseases by Ligands Conjugated to Fluorescent Compounds. US patent: US20140271484A1. January 12, 2016.
29. Mahalingam S, Kularatne SA, Myers CH, *et al.* Evaluation of Novel Tumor-Targeted Near-Infrared Probe for Fluorescence-Guided Surgery of Cancer. *J Med Chem.* 2018; 61; 21: p.9637-9646. DOI:10.1021/acs.jmedchem.8b01115
30. Kalli KR, Oberg AL, Keeney GL, *et al.* Folate receptor alpha as a tumour target in epithelial ovarian cancer. *Gynecol Oncol.* 2008; 108; 3: p.619-626. DOI: 10.1016/j.ygyno.2007.11.020
31. O'Shannessy DJ, Somers EB, Maltzman J, Smale R, Fu YS. Folate receptor alpha (FRA) expression in breast cancer: identification of a new molecular subtype and association with triple negative disease. *Springerplus.* 2012; 28; 1: 22. DOI: 10.1186/2193-1801-1-22
32. Ross JF, Chaudhuri PK, Ratnam R. Differential regulation of folate receptor isoforms in normal and malignant tissues in vivo and in established cell lines. Physiologic and clinical implications. *Cancer.* 1994; 73; 9: p.2432-2443. DOI: 10.1002/1097-0142(19940501)73:9<2432::aid-cncr2820730929>3.0.co;2-s
33. Cheung A, Bax HJ, Josephs DH, *et al.* 2016. Targeting folate receptor alpha for cancer treatment. *Oncotarget*, 2016; 7; 32: p.52553-52574. DOI: 10.18632/oncotarget.9651
34. Scaranti M, Cojocaru E, Banerjee S, Banerji U. Exploiting the folate receptor α in oncology. *Nat Rev Clin Oncol.* 2020; 17; 6: p.349-359. DOI: 10.1038/s41571-020-0339-5

35. DiSaia P, Creasman W, Mannell R, *et al.* Targeted Therapy and Molecular Genetics. *Clinical Gynaecologic Oncology (Ninth Edition)*. Elsevier; 2018.
36. On Target Laboratories. OTL38 for Intra-operative Imaging of Folate Receptor Positive Ovarian Cancer. ClinicalTrials.gov. Identifier: NCT03180307. Updated February 4, 2022. Accessed April 2022. <https://clinicaltrials.gov/ct2/show/NCT03180307>
37. On Target Laboratories. ELUCIDATE: Enabling Lung Cancer Identification Using Folate Receptor Targeting (Elucidate). ClinicalTrials.gov. Identifier: NCT04241315. Updated March 23, 2023. <https://clinicaltrials.gov/ct2/show/NCT04241315>
38. Food and Drug Administration. Approved Drugs: FDA approves pafolacianine for identifying malignant ovarian cancer lesions. <https://www.fda.gov/drugs> [accessed April 2022].
39. Predina JD, Newton A, Xia L, *et al.* An open label trial of folate receptor-targeted intraoperative molecular imaging to localize pulmonary squamous cell carcinomas. *Oncotarget*. 2018; 9; 17: p.13517-13529. DOI: 10.18632/oncotarget.24399
40. Veiseh M, Gabikian P, Bahrami SB, *et al.* Tumour Paint: A Chlorotoxin: Cy5.5 Bioconjugate for Intraoperative Visualization of Cancer Foci. *Cancer Res*. 2007; 67; 14: p.6882-6888. DOI: 10.1158/0008-5472.CAN-06-3948
41. Patil CG, Walker DG, Miller DM, *et al.* Phase 1 Safety, Pharmacokinetics, and Fluorescence Imaging Study of Tozuleristide (BLZ-100) in Adults With Newly Diagnosed or Recurrent Gliomas. *Neurosurgery*. 2019; 85; 4: E641-E649. DOI: 10.1093/neuros/nyz125
42. Blaze Bioscience Inc. Study of Tozuleristide and the Canvas Imaging System in Paediatric Subjects With CNS Tumours Undergoing Surgery. ClinicalTrials.gov. Identifier: NCT03579602. Updated November 14, 2022. <https://clinicaltrials.gov/ct2/show/NCT03579602>
43. Soroceanu L, Gillespie Y, Khazaeli MB, Sontheimer H. Use of chlorotoxin for targeting of primary brain tumours. *Cancer Res*. 1998; 58; 21: p.4871-4879.
44. Ojeda PG, Wang CK, Crail DJ. Chlorotoxin: Structure, activity, and potential uses in cancer therapy. *Biopolymers*. 2016; 106; 1: p.25-36. DOI: 10.1002/bip.22748
45. Peretti M, Angelini M, Savalli N *et al.* Chloride channels in cancer: Focus on chloride intracellular channel 1 and 4 (CLIC1 AND CLIC4) proteins in tumour development and as novel therapeutic targets. *Biochim Biophys Acta*. 2015; 1848; 10: p.2523-2531. DOI: 10.1016/j.bbame.2014.12.012

46. Kittle DS, Mamelak A, Parrish-Novak JE, *et al.* Fluorescence-Guided Tumour Visualization Using the Tumor Paint BLZ-100. *Cureus*. 2014; 6; 9: e210. DOI: 10.7759/cureus.210.
47. Kim K, Cai J, Shuja S, Kuo T, Murnane MJ. Presence Of Activated Ras Correlates With Increased Cysteine Proteinase Activities In Human Colorectal Carcinomas. *Int J. Cancer*. 1998; 79: p.324-333. DOI: 10.1002/(sici)1097-0215(19980821)79:4<324::aid-ijc4>3.0.co;2-x
48. Rudzińska M, Parodi A, Soond SM, *et al.* The Role of Cysteine Cathepsins in Cancer Progression and Drug Resistance. *Int J Mol Sci*. 2019; 20; 14: 3602. DOI: 10.3390/ijms20143602.
49. Lumicell. *Technology Overview*. www.lumicell.com [accessed April 2022].
50. Whitley MJ, Cardona DM, Lazarides AL, *et al.* A mouse-human phase 1 co-clinical trial of a protease-activated fluorescent probe for imaging cancer. *Sci Transl Med*. 2016; 8; 320. DOI: 10.1126/scitranslmed.aad0293
51. Lee DW, Bawendi MG, Ferrer J, inventors: Lumicell Inc, assignee Imaging Agent for Detection Of Diseased Cells. US patent: US9763577B2. September 19, 2017.
52. Whitley M. Preclinical and Clinical Studies of an Investigational Protease-Activated Fluorescent Probe for Cancer Theranostics. [Thesis]. Duke University; 2017.
53. Lumicell Inc. Investigation of Novel Surgical Imaging for Tumour Excision (INSITE). ClinicalTrials.gov. Identifier NCT03686215. Updated December 16, 2022. https://clinicaltrials.gov/ct2/show/NCT03686215.
54. Fox IJ, Brooker LG, Heseltine DW, Essex HE, Wood EH. A tricarbocyanine dye for continuous recording of dilution curves in whole blood independent of variations in blood oxygen saturation. *Proc Mayo Clinic*. 1957; 32; 18; p.478-484.
55. Wheeler HO, Cranston WI, Meltzer JI. Hepatic uptake and biliary excretion of indocyanine green in the dog. *Proc Soc of Exp Biol Med*. 1958; 99; 1: p.11-14. DOI: 10.3181/00379727-99-24229.
56. Norat P, Soldozy S, Elsarrag M, *et al.* Application of Indocyanine Green Videoangiography in Aneurysm Surgery: Evidence, Techniques, Practical Tips. *Front Surg*. 2019; 6; 34. DOI: 10.3389/fsurg.2019.00034.
57. Detter C, Wipper S, Russ D, *et al.* Fluorescent cardiac imaging: a novel intraoperative method for quantitative assessment of myocardial perfusion during graded coronary artery stenosis. *Circulation*. 2007; 116; 9: p.1007-1014. DOI: 10.1161/CIRCULATIONAHA.106.655936

58. Boni L, David G, Mangano A, *et al.* Clinical applications of indocyanine green (ICG) enhanced fluorescence in laparoscopic surgery. *Surg Endosc.* 2015; 29; 7: p.2046-2055. DOI: 10.1007/s00464-014-3895-x
59. Alander JT, Kaartinen I, Laakso A, *et al.* A review of indocyanine green fluorescent imaging in surgery. *Int J of Biomed Imaging.* 2012: 940585. DOI: 10.1155/2012/940585
60. Ergin A, Wang M, Zhang JY, *et al.* The feasibility of real-time in vivo optical detection of blood-brain barrier disruption with indocyanine green. *J of Neurooncol.* 2012; 106; 3: p.551-560. DOI: 10.1007/s11060-011-0711-5
61. Hu Z, Fang C, Li B, *et al.* First-in-human liver-tumour surgery guided by multispectral fluorescence imaging in the visible and near-infrared-I/II windows. *Nat Biomed Eng.* 2020; 4; 3: p. 259-271. DOI: 10.1038/s41551-019-0494-0
62. Shi X, Zhang Z, Zhang Z, *et al.* Near-Infrared Window II Fluorescence Image-Guided Surgery of High-Grade Gliomas Prolongs the Progression-Free Survival of Patients. *IEEE Transactions on Biomed Eng.* 2022; 69; 6: p.1889-1900. DOI: 10.1109/TBME.2021.3130195.
63. Whitney M, Crisp J, Nguyen L, *et al.* Fluorescent peptides highlight peripheral nerves during surgery in mice. *Nat Biotechnol.* 2011; 29; 4: p.352-356. DOI: 10.1038/nbt.1764.
64. Hussain T, Mastrodimos MB, Raju SC, *et al.* Fluorescently Labelled Peptide Increases Identification of Degenerated Facial Nerve Branches during Surgery and Improves Functional Outcome. *PLoS ONE*, 2015; 10; 3: e0119600. DOI: 10.1371/journal.pone.0119600.
65. Antoniadis G, Kretschmer T, Pedro MT, *et al.* Iatrogenic Nerve Injuries. *Dtsch Arztebl Int.* 2014; 111; 16: p.273-279. DOI: 10.3238/arztebl.2014.0273
66. Baibek A, Ucuncu M, Blackburn EA, Bradley M, Lilienkamp A. Wash-free, peptide-based fluorogenic probes for microbial imaging. *Peptide Science.* 2020; 113; 1: e24167. DOI: 10.1002/pep2.24167.

Figure 1. Overview of haemoglobin biosynthesis pathway, showing the major metabolic steps and enzymes (in blue) to form haem prior to its conjugation to a protein to form haemoglobin. In healthy tissue, haem formation has a negative feedback effect on aminolevulinic acid synthase, allowing the cell concentrations of 5-ALA and, by extension, haem to be controlled^{5,6}. In cancerous tissue, a reduced ferrochelatase expression level results in a build-up of the PpIX intermediate that is fluorescent (emits at 635 nm when excited at 405 nm).

Figure 2. Example of the fluorescence imaging capabilities of 5-ALA (administered as 5-ALA hydrochloride) in visualising a high-grade glioma 5-ALA imaging helps tumour identification (in pink) and delineation of surrounding healthy tissue (in blue). Areas of dense, necrotic tissue in the tumour core that are no longer metabolising are unable to generate/accumulate the fluorescent PpIX. Proliferating solid tumour (in A annotated by*) and regions of diffuse tumour infiltration (in B indicated by white arrows) where margins are unclear are demonstrated in the image above¹⁷ (left). Image reproduced from open access article¹⁷ with permission from Frontiers Media.

Figure 3. Chemical structure of EMI-137 showing the disulphide bridges between cysteine residues 4-16 and 6-14. The Cy5** fluorophore (in red), bearing four sulfonate groups to promote solubility, is conjugated to the targeting peptide via a small peptide spacer (GGGK).

Figure 4. Images from colonoscopy of bowel colorectal polyps when the patient has been administered with EMI-137. Images on the left show the comparison of visualisation using standard white light (in the field of view in an endoscopy/colonoscopy) compared to the fluorescent images (in green) showing ‘unseen’ polyps that were not as evident in white light from the application of EMI 137²⁴. Image reproduced from article²⁴ with copyright permission granted from Springer Nature.

Figure 5. Comparison of traditional “white light” imaging and fluorescence imaging (excitation at 650 nm) with an overlay of images of the inflamed oesophagus when EMI-137 was administered IV. The overlay highlights (in green) where EMI-137 has concentrated likely where there is increased c-MET receptor expression²⁷. Image reproduced from open access article²⁷ with permission from Ivyspring International.

Figure 6. Chemical structure of probe OTL38 where a folate-type ligand is conjugated to the SO456 indole-like NIR dye (in red) via a tyrosine residue.

Figure 7. Comparison of *in situ* tumour visualisation of pulmonary squamous cell carcinomas in white light alone (left) and by merge of observed OTL38 fluorescence at 776

nm. Overlaying OTL38 signal provides localisation of FR α ^{+ve} tumour tissue to allow for focused resection of diseased tissue³⁹. Image reproduced from open access article³⁹ with permission from Elsevier.

Figure 8. A-B) injected BLZ-100 on whole mouse brain imaged using a clinical prototype imaging system ‘SIRIS’ system with tumour highlighted; C) whole mouse imaging of IV BLZ-100 with peripheral tumour cells highlighted; D-E) histological staining showing tumour tissue⁴⁶. Image reproduced from open access article⁴⁶ with permission from Cureus.

Figure 9. The structure of the FRET-based LUM015 and the fragments resulting from cathepsin cleavage at the Arg–Lys amide bond. Fragment 1 contains the QSY21-GGR. Fragment 2 is composed of the fluorescent Cy5 dye attached to the 40kD PEG chain via the lysine residue, whilst Fragment 3 is Lys-Cy5 where the PEG chain has been cleaved. Fragment 1 is optically inactive when excited at 649 nm, whilst Fragments 2 and 3 emit at 670 nm.

Figure 10: Comparison of the splenic artery provided by standard white light (left) and ICG fluorescence (right). ICG diluted in saline was administered intravenously and imaged using ICG-Pulsion by Pulsion Medical System. In the presence of ICG, visualisation at 800 nm provides a more readily defined splenic artery outline than white light alone. Image reproduced from open access article⁵⁸ with permission from Springer Nature.

Table 1: Summary of imaging agents discussed in the review (both FDA approved and investigational new drugs) highlighting the disease type, area targeted by probe, structure type, approval status, optical properties and reported dosage.